



Article

Detrital Tourmalines in the Cretaceous–Eocene Julian and Brkini Flysch Basins (SE Alps, Italy and Slovenia)

Davide Lenaz ^{1,*}, Giovanna Garlatti ², Francesco Bernardi ² and Sergio Andò ²¹ Department of Mathematics, Informatics and Geosciences, University of Trieste, 34128 Trieste, Italy² Laboratory for Provenance Studies, Department of Earth and Environmental Sciences, University of Milano-Bicocca, 20126 Milan, Italy; giovanna.garlatti@studenti.units.it (G.G.); francesco.bernardi@phd.units.it (F.B.); sergio.ando@unimib.it (S.A.)

* Correspondence: lenaz@units.it

Abstract: In the SE Alps, two Cretaceous–Eocene flysch basins, Julian and Brkini, filled with turbidite sediments, are present. This study novelly reports heavy mineral assemblage counts and detrital tourmaline characterization for 11 samples. It is possible to define three different groups, characterized by the presence of (1) a clinopyroxene–epidote–low-ZTR (zircon+tourmaline+rutile; 5%) sample association, (2) a high-ZTR (>48%)–garnet–apatite association and (3) a low-ZTR (<40%)–Cr-spinel–garnet association. Detrital tourmalines from both the Julian and Brkini flysch basins are rather similar in composition, associated with metapelites and metapsammites coexisting or not coexisting with an Al-saturating phase, ferric-iron-rich quartz–tourmaline rocks and calc–silicate rocks; however, their number is drastically different. In fact, even if the percentage of heavy minerals is very low and similar in both basins (0.17–1.34% in weight), in the Julian basin, the number of tourmaline crystals is much lower than that in Brkini (1–14 vs. 30–100), suggesting an important change in the provenance area. Interestingly, the presence of a high amount of tourmaline derived from ferric-iron-rich quartz–tourmaline rocks and calc–silicate rocks makes these two basins different from all the Cretaceous flysch basins of Bosnia and the Northern Dinaric zone, where these supplies are missing or very limited.

Keywords: heavy mineral assemblage; tourmaline; flysch basins; Cretaceous–Eocene; Italy; Slovenia

Citation: Lenaz, D.; Garlatti, G.; Bernardi, F.; Andò, S. Detrital Tourmalines in the Cretaceous–Eocene Julian and Brkini Flysch Basins (SE Alps, Italy and Slovenia). *Minerals* **2024**, *14*, 598. <https://doi.org/10.3390/min14060598>

Academic Editors: Jan Golonka, Andrzej Śla0327czka, František Teřák and Georgia Pe-Piper

Received: 2 May 2024

Revised: 30 May 2024

Accepted: 4 June 2024

Published: 7 June 2024



Copyright: © 2024 by the authors. Licensee MDPI, Basel, Switzerland. This article is an open access article distributed under the terms and conditions of the Creative Commons Attribution (CC BY) license (<https://creativecommons.org/licenses/by/4.0/>).

1. Introduction

The Julian and Brkini sedimentary basins in the SE Alps are two nearby Cretaceous–Tertiary basins filled with turbidite sediments. In the past, several studies dealt with their mineralogy in terms of their main constituents, either clay or heavy minerals. As far as concerns the Julian basin, Cr-spinel [1] and HP-LT minerals such as amphibole and omphacitic pyroxene [2] have been found and studied. In the Brkini basin, Refs. [3,4] studied the heavy mineral paragenesis. A more detailed study on Cr-spinel in the Brkini basin was performed by [5], while [6,7] studied garnet, zircon and rutile in both the Julian and Brkini basins.

Even if tourmaline was noticed in [3] in the Brkini basin and is considered an important heavy mineral in provenance studies [8–25], no specific studies have been performed on this mineral in the Julian and Brkini basins. This study would like to fill the gap, and by analyzing the chemistry of detrital tourmaline, would like to verify possible changes in its quantity and typology across space and time.

2. Geological Settings

The Apulian plate formed during the Early Mesozoic, following the break-up of Pangea and the consequent separation of Africa from Eurasia. Later on, during the Jurassic, extensive spreading of the seafloor occurred to the west of and north of the Adria plate.

This caused the Tethys subduction below the eastern border of the Adria promontory. The Vardar Ocean formed by the end of the Jurassic, and in the Early and Middle Cretaceous, the collision of the microplate resulted in two suture zones, from which the Dinarides originated. Finally, in the Late Cretaceous, subduction culminated in continental collision of the Alpine orogenic belts, causing the creation of several foreland basins [26,27]. In the studied area, it is possible to recognize the following basins: Claut and Clauzetto (Upper Paleocene–Lower Eocene) [28]; Julian (Upper Cretaceous–Middle Eocene) [29,30]; Vipava and Pivka (Early Eocene) [3]; Brkini (Lower–Middle Eocene) [31,32]; Istrian and Kvarner (Krk, Pag and Rab Islands) (Middle–Upper Eocene) [33] (Figure 1). Progressive emersion of the land caused the shifting to the SE of the basins so that they were consequently filled, with possible episodes of recycling [32].

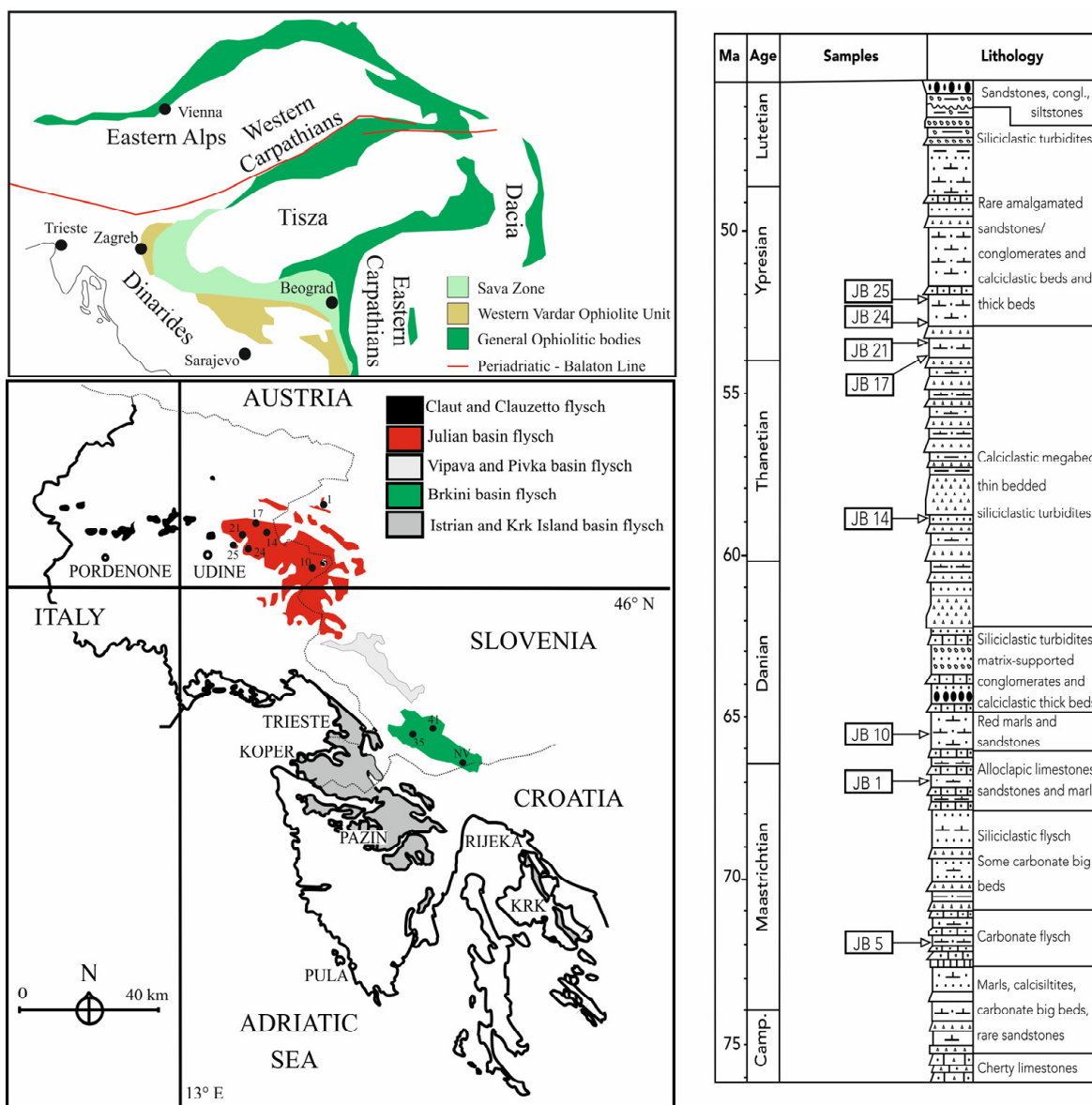


Figure 1. Simplified geological map modified after [34] indicating the main geological units and the main ophiolitic bodies. Flysch deposits of the Southeastern Alps and sample positions within the stratigraphic column. JB1 cannot be considered part of the stratigraphic succession of the Julian basin (see text for details), but it has been located at its correspondent age [35]. No stratigraphic column is available for Brkini basin (see text for details).

The Julian basin (JB; sometimes described as the Slovenian Trough) is a sedimentary basin that has been active from the Maastrichtian (Upper Cretaceous) to the Middle Eocene; it is elongated in the NW–SE direction. According to [30], deposition of the turbiditic sequence was initiated during the Senonian and continued until the early Eocene [29]. The turbiditic sequence is characterized by mixed siliciclastic–carbonate material with a total thickness of about 4000 m. According to [36], siliciclastic turbidites alternated with carbonate strata from the Dinaric carbonate platform during regression so that several carbonate megabeds, such as those of Ioanaz Mt., Staipa Mt., Topli Uorch, Vernasso and Porzus, are present [37–39]. Venturini and Tunis (1992) [28] recognized quartz and calcite as the main constituents; plagioclases, clay minerals and dolomites are minor components, whereas microcline and micas are very rare. Among the lithic fragments, dolostones, limestones, radiolarites, cherts, diabase, sandstones, quartzites, gneisses and low-grade schist are present [28] (Figure 2). These authors classified them as lithic greywacke. Later on, Refs. [40,41] analyzed some of the samples present in this study, confirming the previous classification by [28]. In the JB, Ref. [40] found in all samples chert, limestone and undetermined lithics. No significant changes in the lithics were noticed by [40]. In the BK, Ref. [41] found chert, limestone, marl, schist and undetermined igneous rock fragments.

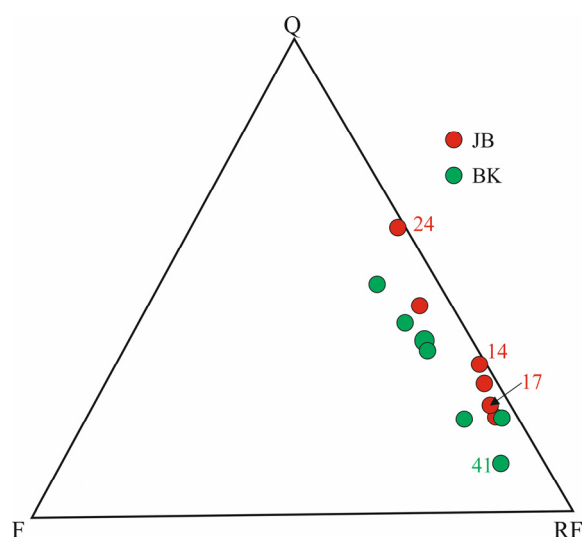


Figure 2. QFL diagram according to [40,41]. Numbers in the figure correspond to samples analyzed in this study too.

Tunis and Venturini (1992) [35] suggested that a possible source of the siliciclastic could be located in the nearby north and northeast areas of the basin, probably in the South Alpine area, implying longitudinal paleocurrents. In the lower Maastrichtian conglomerate at the base of the sequence in Bovec (Slovenia) (JB1), Ref. [42] found and studied about 60 well-sorted volcanic clasts (average diameter of 0.8 cm), with tholeiitic affinities showing similarities with the metabasites from the ophiolitic complexes of the Rhodopes and the Vardar zone. According to [43,44], the Bovec basin was a narrow basin belonging to the Julian nappe. Since the structure is complex and with scarce and laterally discontinuous exposure, it is difficult to locate the exact position of this basin within the regional paleogeography. The Bovec basin was presumably part of the Tolmin basin to the south but may be connected to the Belluno basin in the Southern Alps [43,44]. In the proper Julian basin, by studying the Cr-spinel chemistry, Ref. [1] recognized both peridotitic and volcanic supplies, i.e., mantle (ophiolitic) peridotites and mantle-derived volcanic rocks sensu [45]. Peridotitic spinels are more abundant and are characteristic of suprasubduction-zone harzburgites. The chemical diversities in volcanic spinels suggest multiple sources, including MORB and back-arc-type spinels, as well as oceanic island basalts and island arc tholeiite supplies [1]. A change in the relative percentage between volcanic and peridotitic spinels appears at

about 56 Ma, when volcanic sources increased. Such supplies suggest a provenance from the Inner Dinarides. Towards the top of the sequence, at about 52 Ma, Ref. [2] found actinolite, Mg-hornblende, barroisite and glaucophane associated with omphacite. These minerals are related to the erosion of HP-LT terranes. The paucity of these minerals and the limited extension in time suggest that they derived from probably limited outcrops, exhumed at about 56 Ma during a phase of Dinarides uplift [46]. According to [6], supplies from amphibolite facies rocks and mafic and ultramafic metamorphic rocks are the most important for the garnets in the Julian basin. Moreover, skarns, very low-grade metabasites and ultra-high-temperature metamorphosed calc-silicate granulites are present. Recently, Refs. [47,48] studied the OH defects in detrital quartz crystals from the Julian basin and suggested that the supplies changed from a mixed metamorphic/magmatic (50%–50%) origin in samples older than 56 Ma to an almost exclusive metamorphic supply at the top of the sequence (less than 20% magmatic).

The Brkini basin (BK) occupies a syncline located in SW Slovenia, with an elongated NW–SE shape. Sedimentation was active from the Late Paleocene, and in particular, flyschoid and molassic material filled the basin during the Eocene, at a thickness of about 1000 m [32]. The presence of strong folding and extensive vegetation cover prevent perfect recognition of the stratigraphic sequence, so it has never been wholly described. At the base, clastic deposits overlie Alveolina-bearing limestones with a 78 m thick olistostrome (Lower Eocene) [31]. According to [32], the top of the succession can be attributed to the Middle Eocene. A 100 m thick sequence of siltstones, marls and sandstones in molasse facies closes the succession (Lutetian or post-Lutetian?) [32]. The paleocurrent data are controversial. Orehek (1972, 1991) [3,49] suggested a sediment supply from the SE, while [32] observed transport from the NW. According to [3], within the heavy mineral paragenesis, it is possible to recognize rutile, zircon, tourmaline, garnet, pyrite and other opaque minerals. Among the opaque minerals, Ref. [4] described Cr-spinel and ilmenite, while in the transparent heavy minerals, they also noticed the presence of orthopyroxene. According to [47], the clastic succession is constituted by lithic greywacke. Lenaz et al. (2003) [5] showed that in the Brkini flysch, the Cr-spinels are mainly peridotitic (80%), and their chemistry suggests a provenance from the same areas of those in the Julian basin. Garnets are represented by those originating from amphibolite facies rocks, whereas those from high-grade metabasic rocks are very few. It is interesting to notice that concerning the Bi-type garnets (*sensu* [50]), there are, according to their trace element content, two different types of garnets in the BK. The garnets from the sample BK41 show an Eu/Eu^* ratio higher than 0.1, similar to those present in the JB, while the garnets from the other samples show an Eu/Eu^* ratio lower than 0.1. According to this difference, Ref. [6] ascribed the sample BK41 to the bottom of the sequence and the others to the top.

De Min et al. (2014) [51] studied the whole rock geochemistry of several sandstone samples in the Julian basin, showing that the first strata are chemically influenced by the disaggregation of metamorphic and non-metamorphic rock types related to the ancient Vardar sea closure, where island-arc- and MORB-like-related rock types were generated. Successively, at about 56 Ma, there was strong involvement of continental upper crustal source rocks. Later on, a new upwelling involved the Julian sediments, which, possibly, partly contributed, with recycled materials, to the creation of the Brkini basin. In the latter basin, other protolith rock types begin to be significant.

3. Materials and Methods

Seven samples from the Julian basin were selected according to their stratigraphic age: JB5 is Maastrichtian, JB10 is Danian, JB14 is Thanetian and JB17, JB21, JB24 and JB25 are Ypresian. Three samples from the Brkini basin were selected considering their Cr-spinel and garnet content has been already studied. BK41 is from the base of the sedimentation cycle in Brkini, BK35 is from the top and BKNV represents the molasse facies closing the sedimentation in the basin. JB1 is a Maastrichtian sample that cannot be ascribed to the sequence of the Julian basin, but it is rather close. Major details on it can be found in

the “Discussion” section. The rocks were crushed in a mortar; then, the heavy minerals were concentrated using sieving and heavy liquids (sodium polytungstate $\text{Na}_6(\text{H}_2\text{W}_{12}\text{O}_{40})$) at the Department of Earth and Environmental Sciences of Bicocca University in Milan, according to the procedure in [52]. We analyzed heavy minerals with a broad spectrum of grain sizes between 75 and 300 microns because this was the only type of material available for heavy mineral analysis. About 200 transparent granules were recognized. The analyzed samples are very rich in heavy grains that are opaque and semi-opaque in transmitted light, often weathered, overwhelming the signal of transparent heavy minerals. While recognizing dimensional variety in the observed granules, it was preferred to use the area method to obtain the suite of minerals, applying a procedure that was not time-consuming [53]. In samples in which transparent heavy minerals prevail, the point counting method has often been applied [54], but even this does not completely solve the problem of 2D vision under an optical microscope, and therefore the transformation of frequencies into percentages remains an approximation [54,55]. To minimize the impact of the abundance of opaque and semi-opaque grains, all grains spread in a randomly drawn area on the slide were counted, reconstructing the relative frequency ratios of all the varieties of grains and minerals encountered. Then, for the subsequent areas, only transparent heavy minerals were considered to create a robust dataset, and only at the end was an estimate of the percentages of opaque and semi-opaque granules calculated following the previous relative proportions.

Raman spectra for olivine crystals were collected in the $140\text{--}1900\text{ cm}^{-1}$ spectral range with a Renishaw inVia™ (Wotton-under-Edge, UK) spectrometer equipped with a Leica DM2500 (Wetzlar, Germany) polarizing microscope, a $50\times$ LWD (long working distance) objective, a solid-state 532 nm laser and a grating of 1800 lines/mm. The acquisition time was ~ 15 s, and the spectral resolution was $\pm 1\text{ cm}^{-1}$. Calibration was carried out before each session with the internal standard of a silicon wafer at 520.6 cm^{-1} .

Then, all the tourmalines from every studied separate were hand-picked under the microscope (Table 1). Microprobe analyses were performed at the Milano Statale University using a Superprobe JEOL Jxa-8200 (Tokyo, Japan), a $1\text{ }\mu\text{m}$ beam spot, 15 kV and 5 nA emission. The counting time was 30 s for the peak and 10 s for the background. The following standards were used for the analyses: omphacite USNM 110-697-154 for Na; Martire grossular for Al, Si and Ca; fayalite USNM 85276-143 for Fe; rhodonite for Mn; K-feldspar PSU-Or-1A-113 for K; Olivine (Fo83) USNM 2566-153 for Mg; ilmenite USNM 96189-149 for Ti and pure V, Zn, Cu and Cr. In the presence of zoned crystals, spot analyses were performed on areas with different chemistry.

Table 1. Percentage of heavy minerals and number of tourmalines and zoned tourmalines in the selected samples. Samples are in stratigraphic sequence (bottom to top is oldest to youngest).

	HM Percentage	Number of Tourmalines	Zoned Tourmalines
BKNV	1.11	30	6
BK35	0.44	100	8
BK41	0.69	54	2
JB25	0.52	10	3
JB24	0.47	6	1
JB21	0.30	14	1
JB17	0.76	1	1
JB14	0.27	11	-
JB10	0.41	1	-
JB5	0.16	12	4
JB1	1.34	1	-

The generalized tourmaline structural formula is $XY_3Z_6(T_6O_{18})(BO_3)_3V_3W$, where the most common ions (or vacancy) at each site are $X = Na^{1+}, Ca^{2+}, K^{1+}$ and vacancy; $Y = Fe^{2+}, Mg^{2+}, Mn^{2+}, Al^{3+}, Li^{1+}, Fe^{3+}$ and Cr^{3+} ; $Z = Al^{3+}, Fe^{3+}, Mg^{2+}$ and Cr^{3+} ; $T = Si^{4+}, Al^{3+}$ and B^{3+} ; $B = B^{3+}$; $V = OH^{1-}$ and O^{2-} and $W = OH^{1-}, F^{1-}$ and O^{2-} [56]. The most compositional variability occurs at the X, Y, Z, W and V sites. Tourmaline species are defined in accordance with the dominant valency rule, such that at a relevant site, the dominant ion of the dominant valence state is used for the basis of the nomenclature. To calculate the structural formulae for the tourmaline analyses based on the current International Mineralogical Association nomenclature scheme (IMA-2011; [56]), we used the Microsoft Visual Basic program, WinTcac, by [57]. This software calculates tourmaline analyses both based on 31 O atom normalization as the default and 15 cations and 6 silicons optionally, shares out the recalculated cations at different sites (T, Z, Y and X) and estimates the OH^{1-} and O^{2-} contents at the V site and the OH^{1-}, F^{1-}, Cl^{1-} and O^{2-} contents at the W site, which is a recommended approach because it is appropriate for tourmalines in almost all metamorphic and most igneous rocks [56]. The latter is the approach we adopted. For the chemical analyses, see the Supplementary Data.

4. Results

After separation, we collected an amount of heavy minerals corresponding to about 0.17–1.34 wt.% of the rocks (Table 1).

The heavy mineral assemblage of the studied samples shows that the JB1 sample is very different from all the others, being dominated by a clinopyroxene–epidote–titanite assemblage and with a prevalence of hydrogrossular over other garnets (Table 2; Figure 3). The ZTR value is very low, about 5 wt.% (Figure 3).

Table 2. Number of mineral grains found in the studied samples. Zrn: zircon; Tur: tourmaline; Rt: rutile; Ti Ox: other TiO_2 oxides; Ttn: titanite; Ap: apatite; Mnz: monazite; Ep: epidote; Grt: garnet; Cld: chloritoid; Am: amphibole; Px: pyroxene; Ol: olivine; Spl: Cr-spinel.

	Zrc	Tur	Rt	Ttn	Ti Ox	Ap	Mnz	Px	Act	Ol	Spl	Ep	Cld	Grt	Other	Total
BKNV	14	18	22	2	1	26	1				46			99		229
BK35	25	37	51		1	25		2			28			37		206
BK41	14	23	21	1	4	18		3			45	1	10	66	41	206
JB25	17	15	22			23		2			60	1	1	24		205
JB24	17	14	20	2	3	5		3		1	44		1	45		155
JB21	16	22	33		1	8		5		1	92	1		20		200
JB17	7	4	5			2	1	1			11			9	2	42
JB14	21	24	30	2	3	11		5			87			22		205
JB10	5	3	3					2		2	5			3		23
JB5	31	36	44		2	23		15		1	33			19		206
JB1	2	5	3	32		1		77	3		4	46	1	26		200

The other older samples from JB, JB5 and JB10, as well as BK35, show ZTR values between 48 and 55% in association with garnet and apatite (Figure 3). It is worth noticing that in the JB samples, there are certain amounts of clinopyroxene (augite and diopside), olivine and Cr-spinel that are missing in the BK one. The occurrence of olivine in sedimentary detritus is usually rare due to its lowest stability among all detrital heavy minerals [58]. In order to understand the possible forsterite content of these olivines, Raman analyses were performed on the crystals found. Olivines were analyzed at both the cores and rims, and no compositional changes were noted. According to [59], the dominant feature of the olivine Raman spectrum is a doublet that occurs in the spectral region of $815\text{--}825\text{ cm}^{-1}$

and 838–857 cm^{-1} , showing monotonic shifts following the cation substitution between forsterite and fayalite (Figure 4). This fact allows us to estimate the chemical composition from the Raman spectra. Interestingly, the rare olivine crystals display a different forsterite content. In fact, in JB5, the unique olivine crystal presents a double peak at 820 and 851 cm^{-1} , suggesting a Fo65 composition. In JB10, there are two olivine crystals: one is similar to the one found in JB5, while the second shows a double peak at 823 and 855 cm^{-1} (Fo90). The remaining olivines (JB21 and JB24) are both Fo90. All the other samples are characterized by a ZTR value slightly decreasing with age (from about 40 to 24) and an association mainly comprising Cr-spinel and garnet.

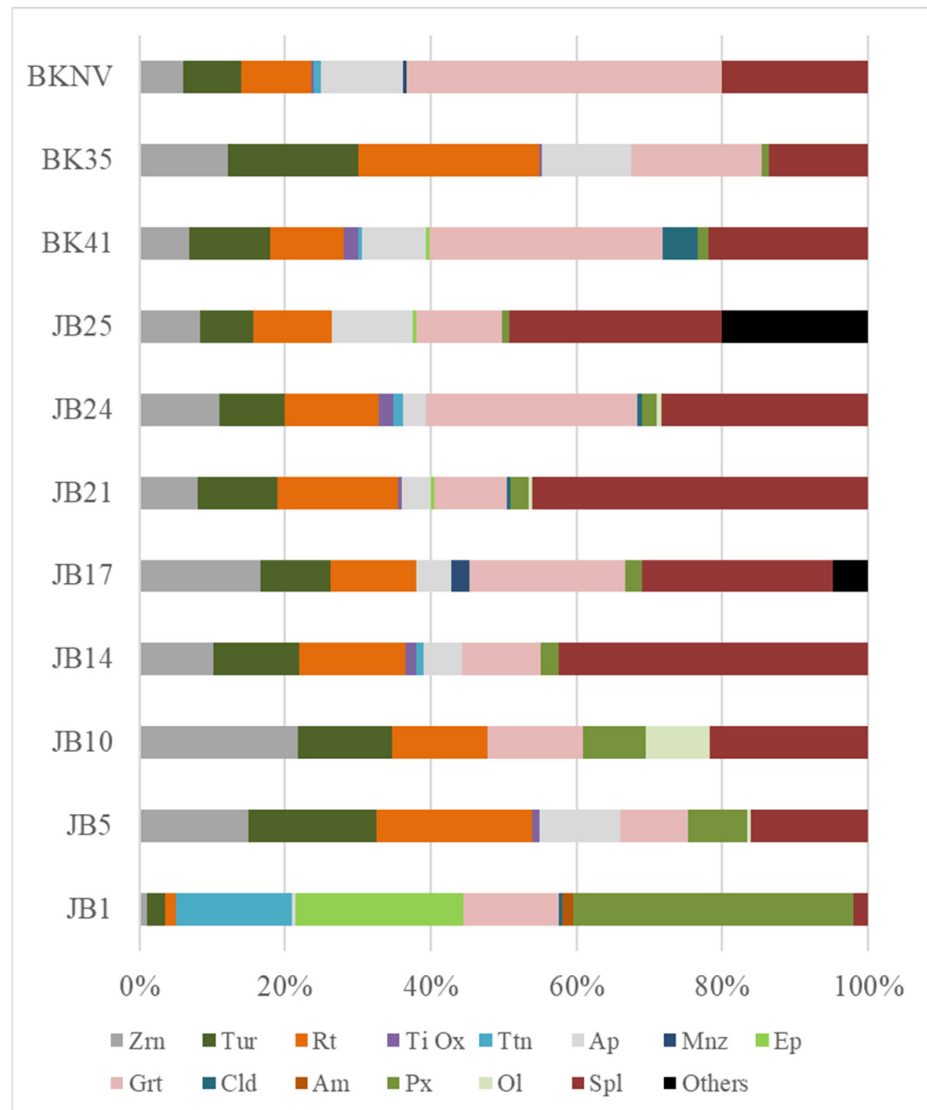


Figure 3. Percentage of heavy minerals in the studied samples according to their stratigraphic position. Labels as in Table 2.

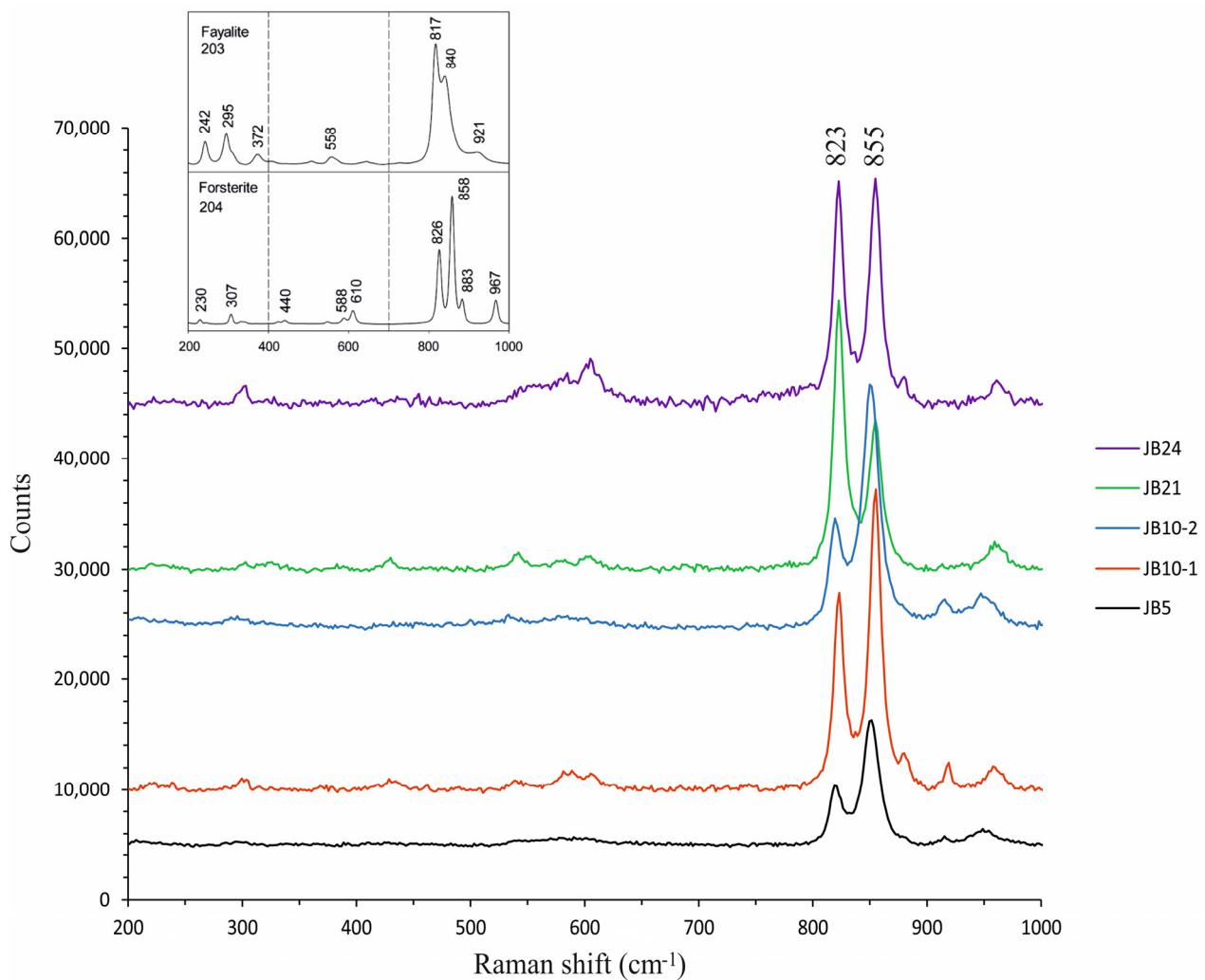


Figure 4. Raman spectra of the olivines found in the JB samples and fayalite and forsterite spectra [59] for comparison.

Considering the heavy mineral percentages, it is possible to see that they are slightly greater in the BK compared to the JB (avg. 0.8 ± 0.3 vs. 0.5 ± 0.4 wt.%). In the JB, there is no trend apart from a slight increase (0.3 to 0.5 wt.%) in its youngest sample (Table 1). The amount of tourmaline is low, 1 to 14 crystals, and there is no trend (Table 1). In the BK, there is a clear inverse correlation between the percentage of heavy minerals and the number of tourmalines; in fact, in BK35, there is the lowest amount of heavy minerals (0.4 wt.%) and the highest number of tourmalines (100), while in the molasse sample BKNV, there is the highest amount of heavy minerals (1.1 wt.%) and the lowest number of tourmalines from the BK (30) (Table 1). Zoned tourmalines are present in all the Ypresian samples from the JB and in the JB5 sample. In the BK, they are always present (Figure 5).

According to [56], for a first classification, the diagram ${}^X\Box / ({}^X\Box + \text{Na} + \text{K})$ vs. $(\text{Mg} / (\text{Mg} + \text{Fe}))$, where \Box is a vacancy, in Figure 6 has been proposed to illustrate the generalized tourmaline species found in our samples. It is possible to see that almost all fall into the dravitic tourmaline field.

In the JB samples, about 9%–10% of the tourmalines fall into the field of schörl, while in the BK, the schörl tourmalines range between 8 (BK35) and 32% (BKNV) (Figure 7). There is only one foititic tourmaline in BKNV. If we consider the rims/overgrowth, almost all are dravitic tourmalines in composition, with minor schörl types present.

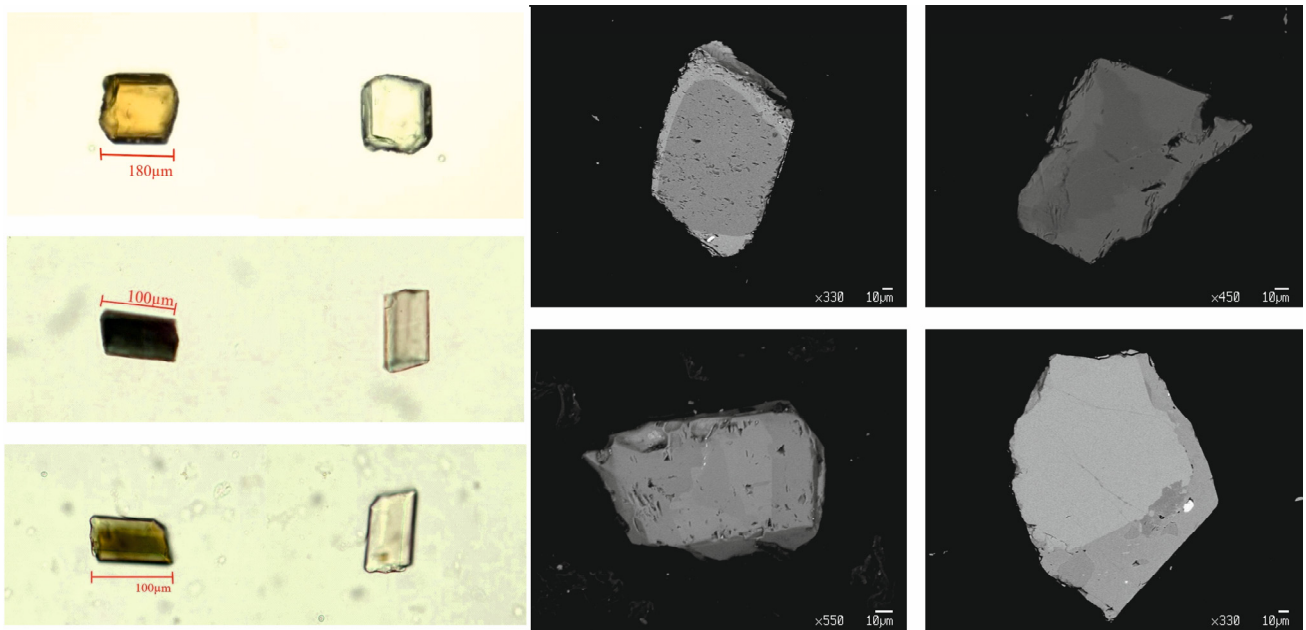


Figure 5. Some images of the tourmalines found in BKNV, BK41, JB25 (top to bottom). To the right, BSE imaging of the zoned tourmalines from JB17, JB24, BK41, BKNV (from the top left moving clockwise).

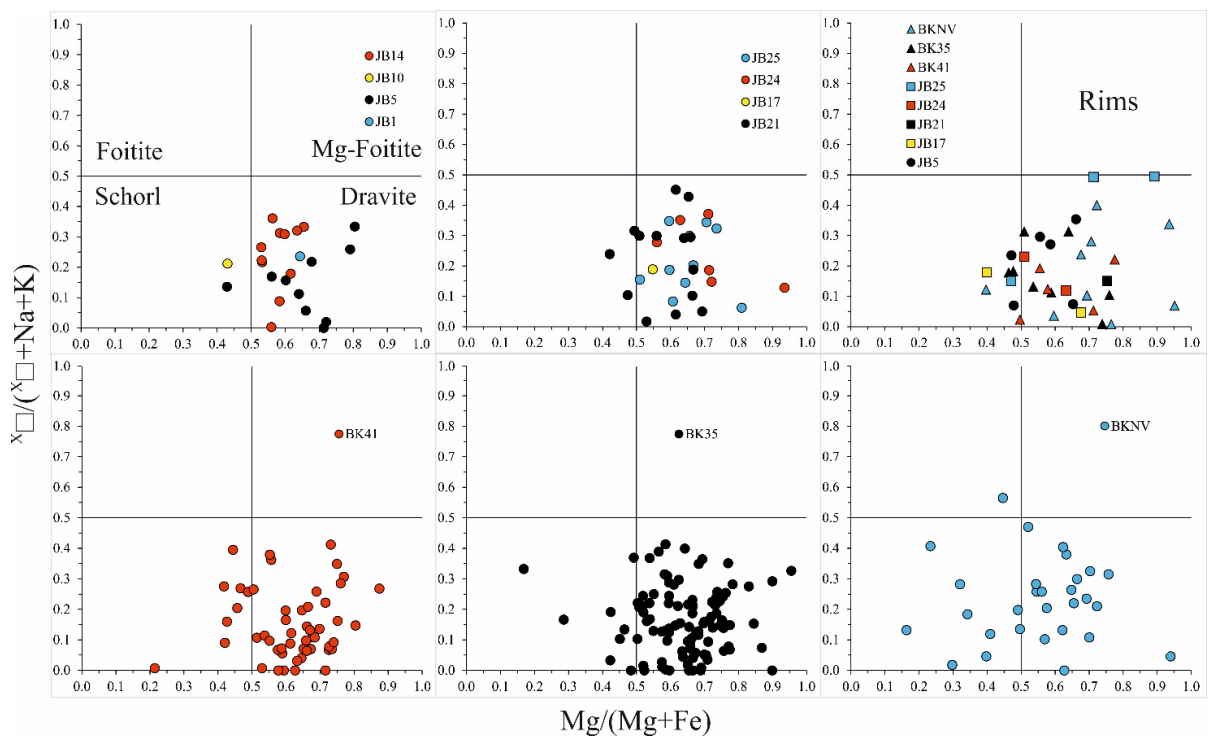


Figure 6. $X_{\square}/(X_{\square}+Na+K)$ vs. $(Mg/(Mg+Fe))$ diagram for the studied tourmalines.

As can be seen above, there is a strong difference between the content of tourmalines within the basins. In the eight JB samples, we found a total amount of 54 tourmalines, while in three samples from the BK, there are 184 tourmalines, even if the percentage of heavy minerals is not so different (0.5 vs. 0.8 wt.%). This fact clearly indicates a substantial change in the provenance of the tourmalines. Considering their compositions, these tourmalines are almost the same; in fact, considering all the tourmalines from the JB and those from BK41 and BK35, about 80%–90% are dravitic tourmalines, with the remnants being schörlitic

ones. Only the youngest sample, BKNV, shows some differences. It is enriched in schörl (30%), and there is one foititic tourmaline (Figure 7).

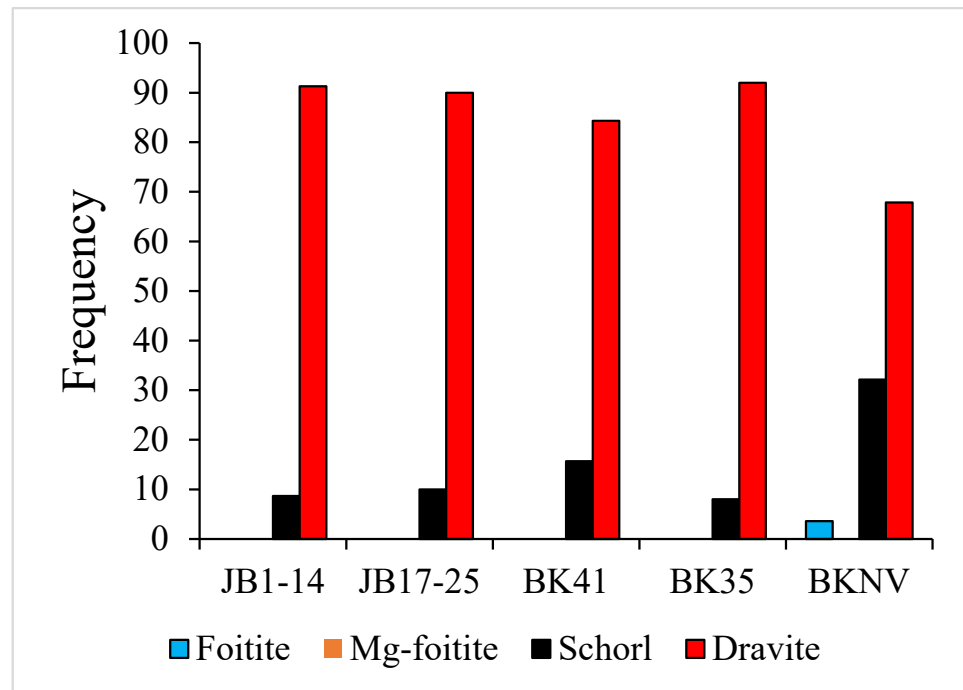


Figure 7. Frequency of the different generalized tourmaline species in the studied samples. Here, the samples of JB are grouped according to their ages. The group JB1-14 includes the samples ranging from Maastrichtian to Thanetian; the group JB17-25 is for Ypresian samples.

To see whether it is possible to better distinguish the tourmalines, the $Al-Al_{50}Fe_{50}-Al_{50}Mg_{50}$ diagram by [60] is often used (Figure 8). This diagram allows us to subdivide the triangle into eight different fields: (1) Li-rich granitoid pegmatites and aplites; (2) Li-poor granitoids and their associated pegmatites and aplites; (3) ferric-iron-rich quartz–tourmaline rocks (hydrothermally altered granites); (4) metapelites and metapsammites coexisting with an Al-saturating phase; (5) metapelites and metapsammites not coexisting with an Al-saturating phase; (6) ferric-iron-rich quartz–tourmaline rocks, calc-silicate rocks and metapelites; (7) low-Ca metaultramafics and Cr, V-rich metasediments; (8) metacarbonates and meta-pyroxenites.

Considering such diagrams, it is easy to see that the main tourmaline supplies are from ferric-iron-rich quartz–tourmaline rocks, calc–silicate rocks and metapelites, followed by metapelites and metapsammites not coexisting with an Al-saturating phase. In the JB, there are two tourmalines from low-Ca metaultramafics and Cr, V-rich metasediments and metacarbonates and meta-pyroxenites. In BK41 and BKNV, there are tourmalines from Li-poor granitoids and their associated pegmatites and aplites, while in BK35 and BKNV, there are a couple of tourmalines from ferric-iron-rich quartz–tourmaline rocks. Similarly to the JB, there are some tourmalines from low-Ca metaultramafics and Cr, V-rich metasediments and metacarbonates and meta-pyroxenites.

As far as concerns the zoned tourmalines, it is possible to recognize two different behaviors. As an example, it is possible to see that almost all of the rims of the tourmalines from BK35 show an increase in iron moving towards the $Al_{50}Fe_{50}$ vertex; on the contrary, the rims of the crystals from BK41 and BKNV move towards the $Al_{50}Mg_{50}$ vertex (Figure 9).

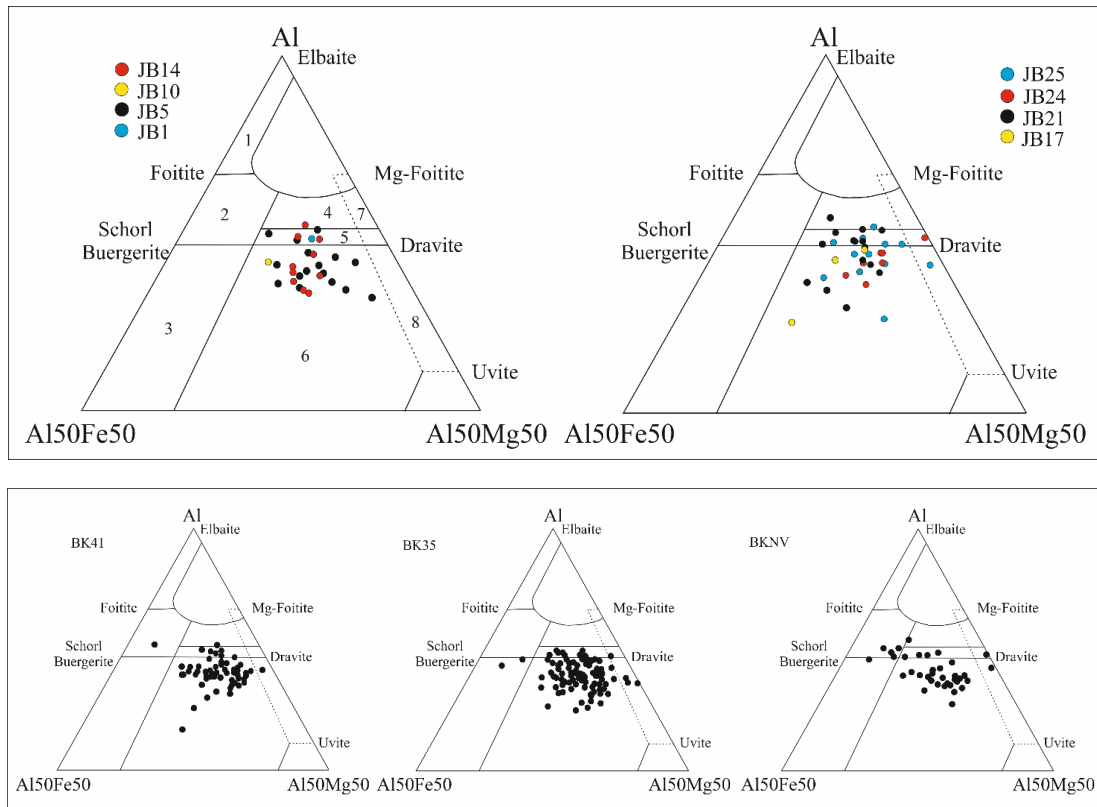


Figure 8. Al-Al₅₀Fe₅₀-Al₅₀Mg₅₀ diagram by [60]. Above: JB samples, below: BK samples. See text for field explanations.

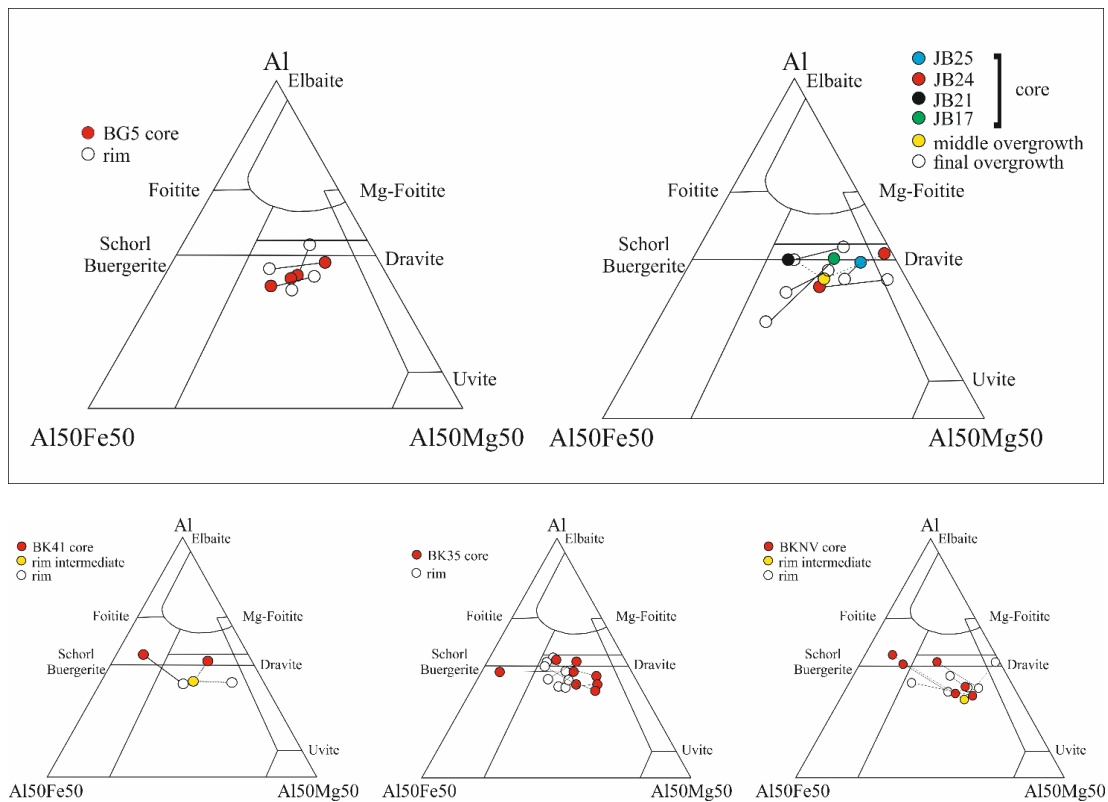


Figure 9. Al-Al₅₀Fe₅₀-Al₅₀Mg₅₀ diagram by [60] for cores and rims of the zoned tourmalines.

5. Discussion

The difference between the heavy mineral assemblage of JB1 and the other samples, as well as the rare presence of olivines, is worthy of an attempt at an explanation, even if it is not the main purpose of this study. In the area close to Bovec (Slovenia), ascribed to the lower Maastrichtian, conglomerate and arenite outcrop. In the conglomerate, [42] found and analyzed sixty well-sorted volcanic clasts. The clasts were variably spilitized. They are classified as tholeiitic, andesitic and transitional basalts, with pheno- and micropheno-crystals of plagioclase, augite ($Wo_{39-42}En_{41-48}Fs_{11-20}$), pigeonite and opaques. Olivine is usually altered into iddingsite. Their chemistry suggested similarities with metabasites from the ophiolitic complexes of the Rhodopes and the Vardar zone and a provenance from quite a delimited and close protolithic area (1–3 hundred kilometers) that did not suffer from sub solidus recrystallization.

In the Dinarides areas, several different Mesozoic flysch basins can be found. The Bosnian flysch forms a ca. 3000 m thick intensely folded deposit of Upper Jurassic to Cretaceous mixed carbonate and siliciclastic sediments [61]. The trench sedimentation was controlled by a dual sediment supply from the sub-ophiolitic high-grade metamorphic soles and from the distal continental margin of the Adriatic plate. The heavy mineral spectra of the Bosnian flysch are overall dominated by Cr-spinel, followed by ZTR, garnet and lesser amounts of apatite, titanite and monazite. Epidote was found in the lower Cretaceous Vranduk formation [61]. No clinopyroxene is present in the heavy mineral assemblage. More northward, the Late Cretaceous consisted of more or less coeval basins, receiving mixed ophiolitic–continental siliciclastic detritus [62].

There, the Maastrichtian Glog formation represents the youngest part of a transgressive Upper Cretaceous alluvial to deep-water succession overlying the rocks of the Paleozoic–Triassic basement wedge, which underwent low-grade Cretaceous metamorphism. In this formation, Ref. [63] found high ZTR, with only minor proportions of heavy minerals such as epidote and garnet. The deep-water turbiditic deposits of the Kravljak formation (Albian–Cenomanian age) are dominated by ZTR but also contain significant Cr-spinel and minor amounts of garnet and apatite, while the Vivodina formation (Maastrichtian) is a deep-water deposit containing ZTR and considerable amounts of Cr-spinel, as well as minor amounts of garnet and epidote/zoisite [64]. Dismembered ophiolites occur in the Dinaride ophiolite zone, related to the open-ocean Tethyan realm, whereas highly dismembered ophiolites occur in the Vardar zone, related to a back-arc basin. According to [65], the ophiolites are predominantly fertile spinel lherzolite (olivine $Fo_{89,9}$) in the western and central parts of the Dinaride ophiolite and Vardar zones, with depleted harzburgites (olivine $Fo_{91,1}$) in their southeastern parts. Cumulate ultramafics (with the same mineralogy as the peridotites but enriched in iron; olivine Fo_{85}) and gabbros are subordinate and are in some places overlain by massive or sheeted dyke complexes, capped by metabasaltic pillow lava. Diabases and dolerites are composed of plagioclase, augite, actinolite and olivine Fo_{70} . These bodies are cross-cut by veins and veinlets filled with epidote, among others. The metamorphic soles of ophiolites are represented by varieties of amphibolites with subordinate pyroxenite schists and scarce eclogites with ultramafic interlayers, which were progressively metamorphosed under the P–T conditions of eclogite, granulite, amphibolite and greenschist facies. Amphibolites related to diabases–dolerites are usually biminerally composed of amphibole and plagioclase, with subordinate epidote.

Within the Alpine domain, since the Oxfordian, several flysch basins have been present in the area, including the Belluno, Bovec, Bled and Tolmin basins [43,66]. As seen above, Refs. [43,44] suggested the Bovec basin was presumably part of the Tolmin basin but may have belonged to the Belluno one. Stefani et al. (2007a) [67] suggested a connection between these two basins as well. However, Ref. [67] showed that in the Belluno basin, the heavy mineral assemblage is rather different from that found in the JB1 sample, being enriched in ZTR (from 10% up to 40%), Cr-spinel, epidote and garnet but completely missing pyroxene and titanite.

Given this evidence, it seems that in our samples, the peridotite ophiolitic source is closer to the NW Dinarides formations, while metamorphic sole supplies are limited. On the contrary, the epidote-bearing metamorphic sole and all the sensu lato basaltic (diabase and dolerite) source rocks that could be related to ophiolites are possibly located to the north of this area and closer to the Bovec and Julian basins. Only later does the presence of ophiolite detritus increase in the heavy mineral assemblage of the Julian and Brkini basins. This can be also detected from the change in the forsteritic content of the rare olivine grains. At the beginning of sedimentation, they are Fo65, with a forsteritic content similar to that found in fresh olivine crystals found in the Triassic magmatism of the Alps [68], while it changes to Fo90 in the younger rocks, a value resembling that of the olivine in the peridotite rocks of the Dinarides (and Cr-spinel is associated).

There are few studies reporting the presence of tourmaline in the surroundings of the studied basins. There are detrital tourmalines in the Paleozoic Slavonian Mountains [69] and in the Late Miocene basins of Northern Croatia [70], but no chemical analyses of these are present. In the Paleozoic Hochwipfel (the Karawanken Mountains between Austria and Slovenia), Ref. [71] reported the presence of detrital tourmaline in both the Eastern and Western Karawanks (Figure 10). The Eastern Karawanken tourmalines show compositions similar to metapelites and metapsammites coexisting with an Al-saturating phase and metapelites and metapsammites not coexisting with an Al-saturating phase (fields 4 and 5 in the diagram by [60]). Those from the Western Karawanks show compositions similar to those from ferric-iron-rich quartz–tourmaline rocks, calc–silicate rocks and metapelites (Field 6 by [60]) but with an Al content lower than that of the here-studied tourmalines (Figure 9). Lužar-Oberiter et al. (2012) [62] studied detrital tourmalines from the Cretaceous basins of the NW Dinarides in Croatia (Oštrc, Bistra, Kravljak, Vivodina and Glog formations). Tourmalines from granitoid sources (Field 2 by [60]) are slightly more common in the Early Cretaceous and Cenomanian than in the Uppermost Cretaceous (Figure 10).

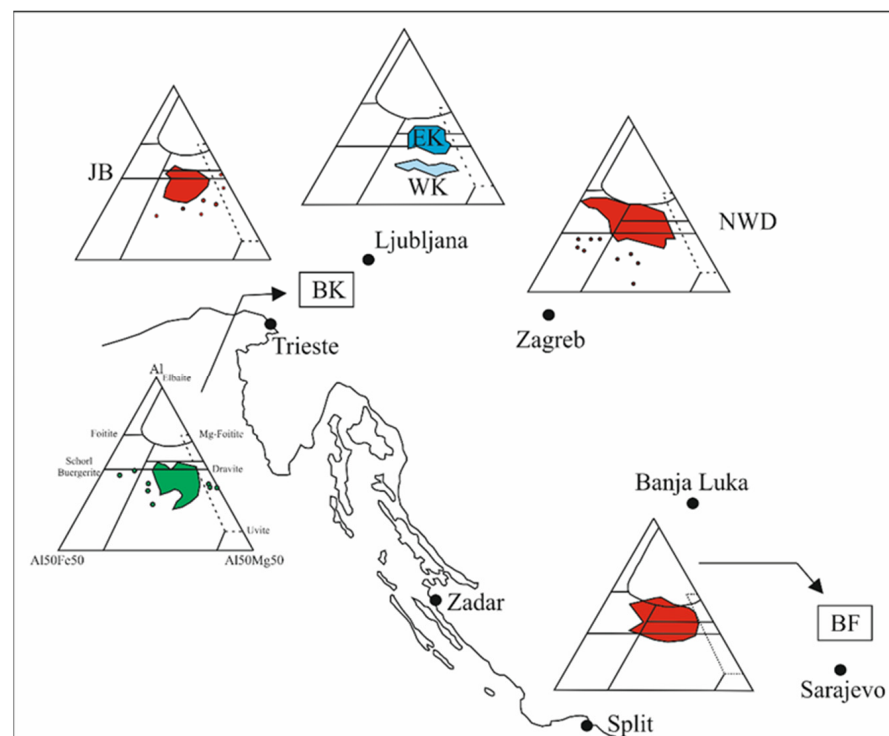


Figure 10. Chemical composition of detrital tourmalines from the Paleozoic Karawanks (blue: Eastern Karawanks, EK; pale blue: Western Karawanks, WK; [71]) and Cretaceous (red; Julian basin: JB, this study; Northwestern Dinarides: NWD, [62]; Bosnian flysch: BF, [61]) and Eocene (green: Brkini, BK, this study) flysch basins.

In the Lower Cretaceous, tourmaline analyses fall within the field of metapelites coexisting with an Al-saturating phase (Oštrc and Bistra), while those from the Cenomanian and Uppermost Cretaceous (Kravljak, Vivodina and Glog) are metapelites not coexisting with an Al-saturating phase (Field 5 by [62]) (Figure 10). In the Cretaceous Bosnian flysch, Ref. [61] found tourmalines falling in fields 4 and 5 in the diagram by [60] (Figure 10). Consequently, it is possible to say that in all these cases, apart from the one from the Western Karawanks, the here-studied tourmalines are different. Balen and Petrinec (2011) [72–75] analyzed tourmalines from Cretaceous Moslavačka granite (Croatia), Permian–Triassic Sopron orthogneiss (Hungary), Cretaceous Pohorje marble (Slovenia) and Permian Velence granite (Hungary), but none of these tourmalines are similar to our detrital ones, so a more precise determination of their provenance is rather impossible at present.

Zoned tourmalines can occur in metapelites, gneisses and pegmatites [76–78], with tourmaline grains displaying distinct asymmetric chemical zoning indicating a diagenetic and/or low-grade metamorphic origin [79]. The formation of rims in tourmaline can be due to the change in the fluid circulating during its crystallization within the source rock or during the diagenetic phase. Pirajino and Smithies (1992) [80] showed that within granite, there is a correlation between the distance from the core to the distal part and the content of MgO, with MgO increasing from endogranitic to proximal, from proximal to intermediate and from intermediate to distal. According to [81,82], tourmaline crystallizes in weakly to moderately acidic solutions but not in alkaline ones. Authigenic tourmaline shows significant X-site vacancies (as a result of low Na content in fluids) and a low Ca content [82–86]. The magnesium content can be very variable, as significant content can be the result of the circulation of marine brines [87,88], while a distinct decrease in Mg and an increase in Fe in the growth direction could be considered an effect of the fluid dilution with respect to Na and Ca over time [88], a decrease in the fluid temperature or, in a metamorphic environment, a decreasing temperature of crystal growth [89]. Considering this, it is hard to define whether the rims originate during their magmatic/metamorphic origin or in a diagenetic environment. However, it is possible that, at least for some samples, these effects could be due to specific diagenetic conditions (Figure 11).

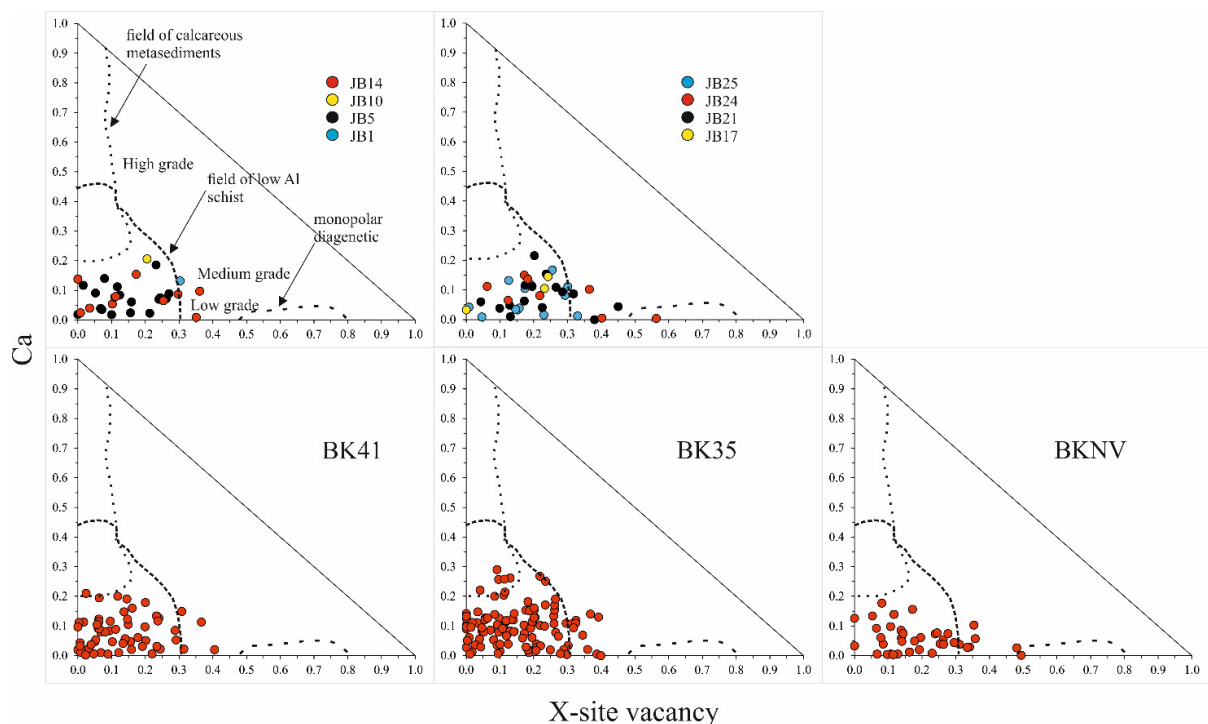


Figure 11. Ca versus X-site vacancy diagram of [84] used for the discrimination of tourmaline from low-Al schists, calcareous metasediment and those from a diagenetic environment.

Tourmaline can be stable under very diverse pressure–temperature conditions, from diagenetic to ultra-high pressure and high-temperature conditions, with the latter showing an increase in Al at the T site and an increase in the Na, Ca and K contents and a decrease in the vacancies at the X site [90–92].

6. Conclusions

The heavy mineral assemblage of the studied samples allows us to define three different groups, characterized by the presence of (i) a clinopyroxene–epidote–low-ZTR (5 wt.%) sample association, (ii) a high ZTR (>48 wt.%)–garnet–apatite association and (iii) a low-ZTR (<40 wt.%)–Cr-spinel–garnet association.

Detrital tourmalines from the Cretaceous to Eocene flysch basins of the Julian and Brkini flysch basins are rather similar in composition, being associated with metapelites and metapsammities coexisting or not coexisting with an Al-saturating phase, ferric-iron-rich quartz–tourmaline rocks and calc–silicate rocks; however, their concentration is drastically different. In fact, in the Julian basin, the number of tourmaline crystals (1–14 vs. 30–100) within a heavy mineral concentrate that is equal in percentage in the two basins is much smaller than in the BK, suggesting an important change in the provenance area of such detritus, similarly to the increase in non-igneous quartz recorded by [48] between the JB and BK basins. The presence of zonation in some grains suggests the possibility of changes in the fluid composition during their crystallization in the source rock, as well as in the diagenetic phase.

Supplementary Materials: The following supporting information can be downloaded at: <https://www.mdpi.com/article/10.3390/min14060598/s1>, Table S1: Chemical analyses of tourmaline crystals analyzed in this study.

Author Contributions: Conceptualization, D.L. and S.A.; methodology, D.L. and S.A.; formal analysis, G.G. and S.A.; writing—original draft preparation, D.L., G.G., F.B. and S.A.; writing—review and editing, D.L. All authors have read and agreed to the published version of the manuscript.

Funding: This research received no external funding.

Data Availability Statement: Data are in the Supplementary Materials.

Acknowledgments: Andrea Risplendente (University of Milano Statale) is kindly acknowledged for his assistance during the microprobe analyses. The three anonymous referees are kindly acknowledged for their comments.

Conflicts of Interest: The authors declare no conflicts of interest.

References

1. Lenaz, D.; Kamenetsky, V.S.; Crawford, A.J.; Princivalle, F. Melt inclusions in detrital spinels from the SE Alps (Italy-Slovenia): A new approach to provenance studies of sedimentary basins. *Contrib. Mineral. Petrol.* **2000**, *139*, 748–758. [CrossRef]
2. Lenaz, D.; Princivalle, F. Detrital high pressure—Low temperature minerals in Lower Eocene deep-sea turbidites of the Julian Alps (NE Italy). *Per. Mineral.* **2002**, *71*, 127–135.
3. Orehek, S. Eocenski fliš pivške kotline in Brkinov. In *7th Kongres Geologov SFRJ, Predavanija*; University of Zagreb: Zagreb, Croatia, 1972; pp. 252–270. (In Slovenian)
4. Lenaz, D.; Alberti, A.; Tunis, G.; Princivalle, F. A heavy mineral association and its paleogeographic implications in the Eocene Brkini Flysch Basin (Slovenia). *Geol. Carpathica* **2001**, *52*, 239–245.
5. Lenaz, D.; Kamenetsky, V.; Princivalle, F. Cr-spinel supply in the Brkini, Istrian and Krk Island flysch basins (Slovenia, Italy and Croatia). *Geol. Mag.* **2003**, *140*, 335–372. [CrossRef]
6. Lenaz, D.; Mazzoli, C.; Velicogna, M.; Princivalle, F. Trace and Rare Earth Elements chemistry of detrital garnets from SE Alps and Outer Dinarides flysch basins: An important tool to better define the source areas of sandstones. *Mar. Pet. Geol.* **2018**, *98*, 653–661. [CrossRef]
7. Velicogna, M. Zircon Dating and Trace Element Content of Transparent Heavy Minerals in Sandstones from the NE Alps and Outer Dinarides Flysch Basins. Ph.D. Thesis, University of Trieste, Trieste, Italy, 2020; 194p. Unpublished.
8. Kowal-Linka, M.; Stawikowski, W. Garnet and tourmaline as provenance indicators of terrigenous material in epicontinental carbonates (Middle Triassic, S Poland). *Sediment. Geol.* **2013**, *291*, 27–47. [CrossRef]

9. Salata, D. Heavy minerals as detritus provenance indicators for the Jurassic pre-Callovia palaeokarst infill from the Czatkowice Quarry (Kraków–Wieluń Upland, Poland). *Geol. Q.* **2013**, *57*, 537–550.
10. Salata, D. Detrital tourmaline as an indicator of source rock lithology: An example from the Ropianka and Menilite formations (Skole Nappe, Polish Flysch Carpathians). *Geol. Q.* **2014**, *58*, 19–30. [[CrossRef](#)]
11. Stern, G.; Wagreich, M. Provenance of the Upper Cretaceous to Eocene Gosau Group around and beneath the Vienna Basin (Austria and Slovakia). *Swiss J. Geosci.* **2013**, *106*, 505–527. [[CrossRef](#)]
12. Vdačnỳ, M.; Bačík, P. Provenance of the Permian Malužiná Formation sandstones (Malé Karpaty Mountains, Western Carpathians): Evidence of garnet and tourmaline mineral chemistry. *Geol. Carpathica* **2015**, *66*, 83–97. [[CrossRef](#)]
13. Bónová, K.; Bóna, J.; Kovačik, M.; Laurinc, D. Heavy minerals from sedimentary rocks of the Malcov Formation and their palaeogeographic implications for evolution of the Magura Basin (Western Carpathians, Slovakia) during the Late Eocene–Late Oligocene. *Geol. Q.* **2016**, *60*, 675–694. [[CrossRef](#)]
14. Bónová, K.; Bóna, J.; Kovačik, M.; Mikuš, T. Heavy minerals and exotic pebbles from the Eocene flysch deposits of the Magura Nappe (Outer Western Carpathians, eastern Slovakia): Their composition and implications on the provenance. *Turk. J. Earth Sci.* **2018**, *27*, 64–88. [[CrossRef](#)]
15. Bónová, K.; Jafarzadeh, M.; Bóna, J.; Mikuš, T.; Anjerdi, J.; Najafzadeh, A.; Mahari, R. Constraints of rare detrital V-rich tourmaline and rutile on late Devonian palaeogeographic reconstruction in the Azarbaijan district, NW Iran. *J. Asian Earth Sci.* **2021**, *221*, 104943. [[CrossRef](#)]
16. Cardona, A.; Valencia, V.A.; Lotero, A.; Villafañez, Y.; Bayona, G. Provenance of middle to late Palaeozoic sediments in the northeastern Colombian Andes: Implications for Pangea reconstruction. *Int. Geol. Rev.* **2016**, *58*, 1914–1939. [[CrossRef](#)]
17. Shi, G.; Wang, H.; Huang, C.; Yang, S.; Song, G. Provenance and tectonic setting of middle-upper Devonian sandstones in the Qinling Orogen (Shanyang area): New insights from geochemistry, heavy minerals and tourmaline chemistry. *Tectonophysics* **2016**, *688*, 11–25. [[CrossRef](#)]
18. Shi, G.; Huang, C.; Xu, S.; Ge, W.; Zhang, Y.; Shi, W. Source to sink systems of the upper Permian Longtan formation in the lower Yangtze region, China: New insights from detrital monazite U–Pb ages and heavy mineral chemistry. *Mar. Pet. Geol.* **2021**, *126*, 104928. [[CrossRef](#)]
19. Li, L.; Wu, C.; Yu, X. Cenozoic evolution of the Altyn Tagh and East Kunlun fault zones inferred from detrital garnet, tourmaline and rutile in southwestern Qaidam Basin (Northern Tibetan Plateau). *Basin Res.* **2018**, *30*, 35–58. [[CrossRef](#)]
20. Bellová, S.; Aubrecht, R.; Mikuš, T. First results of systematic provenance analysis of the heavy mineral assemblages from the Albian to Cenomanian exotic flysch deposits of the Klappe Unit, Tatricum, Fatricum and some adjacent units. *Acta Geol. Slovaca* **2018**, *10*, 45–64.
21. Farnsworth-Pinkerton, S.; McMillan, N.J.; Dutrow, B.L.; Henry, D.J. Provenance of detrital tourmalines from Proterozoic metasedimentary rocks in the Picuris Mountains, New Mexico, using Laser-Induced Breakdown Spectroscopy. *J. Geosci.* **2018**, *63*, 193–198. [[CrossRef](#)]
22. Kotowski, J.; Nejbort, K.; Olszewska-Nejbort, D. Tourmalines as a Tool in Provenance Studies of Terrigenous Material in Extra-Carpathian Albian (Uppermost Lower Cretaceous) Sands of Miechów Synclinorium, Southern Poland. *Minerals* **2020**, *10*, 917. [[CrossRef](#)]
23. Guo, R.; Hu, X.; Garzanti, E.; Lai, W. Boron isotope composition of detrital tourmaline: A new tool in provenance analysis. *Lithos* **2021**, *400–401*, 106360. [[CrossRef](#)]
24. Jafarzadeh, M.; Bónová, K.; Mikuš, T.; Bóna, J.; Rezaei-Kahkhaei, M.; Taheri, A. Tourmaline and rutile geochemistry in the Early–Middle Devonian sandstones of the Padeha Formation, Alborz Range, Northern Iran. *Geol. J.* **2021**, *56*, 4645–4666. [[CrossRef](#)]
25. Liu, S.; Zhang, G.; Li, H. Detrital zircon, monazite and tourmaline reveal the magmatic and metamorphic history of the Himalayan orogen from Archean to present. *Lithos* **2023**, *436–437*, 106949. [[CrossRef](#)]
26. Robertson, A.H.F.; Karamata, S. The role of subduction-accretion processes in the tectonic evolution of the Mesozoic Tethys in Serbia. *Tectonophysics* **1994**, *234*, 73–94. [[CrossRef](#)]
27. Channell, J.E.T.; Kozur, H.W. How many oceans? Meliata, Vardar, and Pindos oceans in Mesozoic Alpine paleogeography. *Geology* **1997**, *25*, 183–186. [[CrossRef](#)]
28. Venturini, S.; Tunis, G. La composizione dei conglomerati cenozoici del Friuli: Dati preliminary. *Studi Geol. Camerti* **1992**, *CROP 1–1A*, 285–295. (In Italian)
29. Tunis, G.; Pirini Radrižani, C. Flyschoid deposits of Goriška Brda (Collio) between Soca (Isonzo) river and Idrija (Iudrio) river—Facies and paleoenvironments. *Geologija* **1987**, *30*, 123–148.
30. Ogorelec, B.; Šribar, L.; Buser, S. O litologiji in biostratigrafiji volcanskega apnenca. *Geologija* **1976**, *19*, 126–151. (In Slovenian)
31. Pavlovec, R.; Knez, M.; Drobne, K.; Pavšič, J. Profiles: Košana, Sv. Trojica and Leskovec; the disintegration of the carbonate platform. In *Field Trip Guidebook; IGCP Project 286—Early Paleogene Benthos, 2nd Meeting Postojna*; University of Ljubljana: Ljubljana, Slovenia, 1991; pp. 69–72.
32. Tunis, G.; Venturini, S. L’Eocene delle Prealpi Carniche, dell’altipiano di Brkini e dell’Istria: Precisazioni biostratigrafiche e paleoambientali. *Nat. Nascosta* **1996**, *13*, 40–49. (In Italian)
33. Magdalenčić, Z. Sedimentologija fliških naslaga srednje istre (Sedimentology of central Istria flysch deposits). *Acta Geol. Zagreb* **1972**, *7/2*, 1–100, (In Croatian with English Summary).

34. Ustaszewski, K.; Kounov, A.; Schmid, S.M.; Schaltegger, U.; Krenn, E.; Frank, W.; Fügenschuh, B. Evolution of the Adria-Europe plate boundary in the northern Dinarides: From continent-continent collision to back-arc extension. *Tectonics* **2010**, *29*, TC6017. [[CrossRef](#)]
35. Tunis, G.; Venturini, S. Evolution of the Southern Margin of the Julian Basin with emphasis on the megabeds and turbidites sequence of the Southern Julian Prealps (NE Italy). *Geol. Croat.* **1992**, *45*, 127–150.
36. Miklavič, B.; Rožič, B. The onset of Maastrichtian basinal sedimentation on Mt. Matajur, NW Slovenia. *Mater. Geoenviron.* **2008**, *55*, 199–214.
37. Tunis, G.; Venturini, S. Nuove osservazioni stratigrafiche sul Mesozoico delle Valli del Natisone (Friuli orientale). *Gortania* **1987**, *8*, 17–68.
38. Ogata, K.; Pogačnik, Ž.; Pini, G.A.; Festa, A.; Camerlenghi, A.; Rebesco, M. The carbonate mass transport deposits of the Paleogene Friuli Basin (Italy/Slovenia): Internal anatomy and inferred genetic processes. *Marine Geol.* **2014**, *356*, 88–110. [[CrossRef](#)]
39. Ogata, K.; Pogačnik, Ž.; Tunis, G.; Pini, G.A.; Festa, A.; Senger, K. A geophysical-geochemical approach to the study of the Paleogene Julian-Slovenian Basin “Megabeds” (Southern Alps-Northwestern Dinarides, Italy/Slovenia). *Geosciences* **2019**, *9*, 155. [[CrossRef](#)]
40. Bertolla, A. Litologie Arenacee della Successione Flyschoida del Bacino Giulio: Significato della Cromite e dei Parametri Petrochimici. Master’s Thesis, University of Trieste, Trieste, Italy, 1997; 91p. Unpublished.
41. Cigna, E. Litologie Arenacee della Successione del Flysch di Clauzetto (Prealpi Carniche) e del Flysch del Brkini (Slovenia Occidentale): Significato della Cromite e dei Parametri Petrochimici. Master’s Thesis, University of Trieste, Trieste, Italy, 1997; 102p. Unpublished.
42. De Min, A.; Rosset, A.; Tunis, G.; Kocmann, C.; Tosone, A.; Lenaz, D. Igneous rock clasts from the Maastrichtian Bovec flysch (Slovenia): Petrology and geodynamic aspects. *Geol. Carpathica* **2007**, *58*, 169–179.
43. Goričan, Š.; Košir, A.; Rožič, B.; Šmuc, A.; Gale, L.; Kukoč, D.; Celarc, B.; Črne, A.E.; Kolar-Jurkovšek, T.; Placer, L.; et al. Mesozoic deep-water basins of the eastern Southern Alps (NW Slovenia). *J. Alp. Geol.* **2012**, *54*, 101–143.
44. Goričan, Š.; Žibret, L.; Košir, A.; Kukoč, D.; Horvat, A. Stratigraphic correlation and structural position of Lower Cretaceous flysch-type deposits in the eastern Southern Alps (NW Slovenia). *Int. J. Earth Sci.* **2018**, *107*, 2933–2953. [[CrossRef](#)]
45. Kamenetsky, V.S.; Crawford, A.J.; Meffre, S. Factors controlling chemistry of magmatic spinel: An empirical study of associated olivine, Cr-spinel and melt inclusions from primitive rocks. *J. Petrol.* **2001**, *42*, 655–671. [[CrossRef](#)]
46. Lawrence, S.R.; Tari-Kovačić, V.; Gjukić, B. Geological evolution model of the Dinarides. *Nafta* **1995**, *46*, 103–113.
47. Bernardi, F.; Skogby, H.; Lenaz, D. OH-defects in detrital quartz grains from the Julian Basin (NE Italy and Slovenia): A Fourier-Transform Infrared study. *Geosciences* **2022**, *12*, 90, Correction in *Geosciences* **2023**, *13*, 127. [[CrossRef](#)]
48. Bernardi, F. Quartz in Sedimentary Rocks: OH-Defects and Trace Elements for Provenance Studies. Ph.D. Thesis, University of Trieste, Trieste, Italy, 2024; 183p. Unpublished.
49. Orehek, S. Palaeotransport of SW Slovenian flysch. In *Field Trip Guidebook; IGCP Project 286—Early Paleogene Benthos*, 2nd Meeting Postojna; University of Ljubljana: Ljubljana, Slovenia, 1991; pp. 27–31.
50. Mange, M.A.; Morton, A.C. Geochemistry of heavy minerals. In *Developments in Sedimentology, Volume: Heavy Minerals in Use*; Mange, M.A., Wright, D.T., Eds.; Elsevier: Amsterdam, The Netherlands, 2007; Volume 58, pp. 345–391.
51. De Min, A.; Princivalle, F.; Lenaz, D. Geochemistry of the Late Mesozoic—Early Cenozoic turbidites from the NE part of the Adria microplate. *Per. Mineral.* **2014**, *83*, 141–158. [[CrossRef](#)]
52. Andò, S. Gravimetric separation of heavy minerals in sediments and rocks. *Minerals* **2020**, *10*, 273. [[CrossRef](#)]
53. Garzanti, E.; Andò, S. Heavy Minerals for Junior Woodchucks. *Minerals* **2019**, *9*, 148. [[CrossRef](#)]
54. Stutenbecker, L.; Krieg, D.; Djahansouzi, A.; Glotzbach, C.; Falkowski, S.; Adolffs, T.; Sindern, S.; Hinderer, M. How to Quantify Heavy Mineral Fertility from Point-Counting Data. *J. Geophys. Res. Earth Surf.* **2024**, *129*, e2023JF007545. [[CrossRef](#)]
55. Schöning, J. Heavy-Mineral Grain Counting: Counting Techniques, Error Estimation, and the Number of Grains to be Counted. *J. Geophys. Res. Earth Surf.* **2024**, *129*, e2023JF007337. [[CrossRef](#)]
56. Henry, D.J.; Novák, M.; Hawthorne, F.C.; Ertl, A.; Dutrow, B.L.; Uher, P.; Pezzotta, F. Nomenclature of the tourmaline-super group minerals. *Am. Mineral.* **2011**, *96*, 895–913. [[CrossRef](#)]
57. Yavuz, F.; Karakaya, N.; Yildirim, D.K.; Karakaya, M.Ç.; Kumral, M. A Windows program for calculation and classification of tourmaline-super group (IMA-2011). *Comput. Geosci.* **2014**, *63*, 70–87. [[CrossRef](#)]
58. Morton, A.C.; Hallsworth, C.R. Stability of heavy detrital minerals during burial diagenesis. In *Developments in Sedimentology, Volume: Heavy Minerals in Use*; Mange, M.A., Wright, D.T., Eds.; Elsevier: Amsterdam, The Netherlands, 2007; Volume 58, pp. 215–245.
59. Kuebler, K.E.; Jolliff, B.L.; Wang, A.; Haskin, L.A. Extracting olivine (Fo-Fa) compositions from Raman spectral peak positions. *Geochim. Cosmochim. Acta* **2006**, *70*, 6201–6222. [[CrossRef](#)]
60. Henry, D.J.; Guidotti, C.V. Tourmaline as a petrogenetic indicator mineral: An example from the staurolite-grade metapelites of NW Maine. *Am. Mineral.* **1985**, *70*, 1–15.
61. Mikes, T.; Christ, D.; Petri, R.; Dunkl, I.; Frei, D.; Baldi-Beke, M.; Reitner, J.; Wemmer, K.; Hrvatović, H.; von Eynatten, H. Provenance of the Bosnian Flysch. *Swiss J. Geosci.* **2008**, *101* (Suppl. 1), S31–S54. [[CrossRef](#)]
62. Lužar-Oberiter, B.; Mikes, T.; Dunkl, I.; Babić, L.; von Eynatten, H. Provenance of Cretaceous synorogenic sediments from the NW Dinarides (Croatia). *Swiss J. Geosci.* **2012**, *105*, 377–399. [[CrossRef](#)]
63. Crnjaković, M. Maastrichtian flysch sediments in the south-west part of Mt. Medvednica. *Geol. Vjesnik* **1981**, *34*, 47–61. (In Croatian with English Summary).

64. Zupanič, J. Non-carbonate detritus from arenite sediments of Maastrichtian Vivodina Flysch (Žumberak, Western Dinarides). *Geol. Vjesnik* **1981**, *34*, 109–120. (In Croatian with English Summary).
65. Pamić, J.; Tomljenović, B.; Balen, D. Geodynamic and petrogenetic evolution of Alpine ophiolites from the Central and NW Dinarides: An overview. *Lithos* **2002**, *65*, 113–142. [[CrossRef](#)]
66. Stefani, C.; Fellin, M.G.; Zattin, M.; Zuffa, G.G.; Dalmonte, C.; Mancin, N.; Zanferrari, A. Provenance and paleogeographic evolution in a multi-source foreland: The Cenozoic Venetian-Friulian Basin (NE Italy). *J. Sediment. Res.* **2007**, *77*, 867–887. [[CrossRef](#)]
67. Stefani, C.; Zattin, M.; Grandesso, P. Petrography of Paleogene turbiditic sedimentation in northeastern Italy. In *Sedimentary Provenance and Petrogenesis: Perspectives from Petrography and Geochemistry: Geological Society of America Special Paper*; Arribas, J., Critelli, S., Johnsson, M.J., Eds.; Geological Society of America: Boulder, CO, USA, 2007; Volume 420, pp. 37–55. [[CrossRef](#)]
68. De Min, A.; Velicogna, M.; Ziberna, L.; Chiaradia, M.; Alberti, A.; Marzoli, A. Triassic magmatism in the European Southern Alps as an early phase of Pangea break-up. *Geol. Mag.* **2020**, *157*, 1800–1822. [[CrossRef](#)]
69. Biševac, V.; Krenn, E.; Finger, F.; Lužar-Oberiter, B.; Balen, D. Provenance of Paleozoic very low- to low-grade metasedimentary rocks of South Tisia (Slavonian Mountains, Radlovac Complex, Croatia). *Geol. Carpathica* **2013**, *64*, 3–22. [[CrossRef](#)]
70. Matošević, M.; Marković, F.; Bigunac, D.; Šuica, S.; Krizmanić, K.; Perković, A.; Kovačić, M.; Pavelić, D. Petrography of the Upper Miocene sandstones from the Northern Croatian Basin: Understanding the genesis of the largest reservoirs in the southern part of the Pannonian Basin system. *Geol. Carpathica* **2023**, *74*, 155–179. [[CrossRef](#)]
71. Kutterolf, S.; Diener, R.; Schacht, U.; Krawinkel, H. Provenance of the Carboniferous Hochwipfel Formation (Karawanken Mountains, Austria/Slovenia)—Geochemistry versus petrography. *Sediment. Geol.* **2008**, *203*, 246–266. [[CrossRef](#)]
72. Balen, D.; Petrinc, Z. Contrasting tourmaline types from peraluminous granites: A case study from Moslavačka Gora (Croatia). *Mineral. Petrol.* **2011**, *102*, 117–134. [[CrossRef](#)]
73. Spránitz, T.; Józsa, S.; Kovács, Z.; Váczi, B.; Török, K. Magmatic and metamorphic evolution of tourmaline-rich rocks of the Sopron area, Eastern Alps (W-Hungary). *J. Geosci.* **2018**, *63*, 175–191. [[CrossRef](#)]
74. Miler, M.; Mašera, T.; Zupančič, N.; Jarc, S. Characteristics of minerals in Slovenian marbles. *Geologija* **2019**, *62*, 175–187. [[CrossRef](#)]
75. Fehér, B.; Zajzon, N. Tourmalines of the Velence Granite Formation and the surrounding contact slate, Velence Mountains, Hungary. *Centr. Eur. Geol.* **2021**, *64*, 38–58. [[CrossRef](#)]
76. Keller, P.; Roda Robles, E.; Pesquera Pérez, A.; Fontan, F. Chemistry, paragenesis and significance of tourmaline in pegmatites of the Southern Tin Belt, central Namibia. *Chem. Geol.* **1999**, *158*, 203–225. [[CrossRef](#)]
77. Tindle, A.G.; Breaks, F.W.; Selway, J.B. Tourmaline in petalite-subtype granitic pegmatites: Evidence of fractionation and contamination from the Pakeagama lake and Separation lake areas of northwestern Ontario, Canada. *Can. Mineral.* **2002**, *40*, 753–788. [[CrossRef](#)]
78. van Hinsberg, V.J.; Schumacher, J.C.; Kearns, S.; Mason, P.R.D.; Franz, G. Hourglass sector zoning in metamorphic tourmaline and resultant major and trace-element fractionation. *Am. Mineral.* **2006**, *91*, 717–728. [[CrossRef](#)]
79. Henry, D.J.; Dutrow, B.L. Metamorphic tourmaline and its petrologic applications. In *Boron: Mineralogy, Petrology, and Geochemistry, Reviews in Mineralogy*; Grew, E.S., Anovitz, L.M., Eds.; Mineralogical Society of America: Chantilly, VA, USA, 1996; Volume 33, pp. 503–557.
80. Pirajno, F.; Smithies, R.H. The FeO/(FeO+MgO) ratio of tourmaline: A useful indicator of spatial variations in granite-related hydrothermal mineral deposits. *J. Geochem. Explor.* **1992**, *42*, 371–381. [[CrossRef](#)]
81. Frondel, C.; Collette, R.L. Synthesis of tourmaline by reaction of mineral grains with NaCl-H₃BO₃ solution, and its implications in rock metamorphism. *Am. Mineral.* **1957**, *42*, 754–758.
82. Morgan, G.B.; London, D. Experimental reactions of amphibolite with boron bearing aqueous fluids at 200 MPa: Implications for tourmaline stability and partial melting in mafic rocks. *Contrib. Mineral. Petrol.* **1989**, *102*, 281–297. [[CrossRef](#)]
83. von Goerne, G.; Franz, G.; Heinrich, W. Synthesis of tourmaline solid solutions in the system Na₂O-MgO-Al₂O₃-SiO₂-B₂O₃-H₂O-HCl and the distribution of Na between tourmaline and fluid at 300 to 700 °C and 200 MPa. *Contrib. Mineral. Petrol.* **2001**, *141*, 160–173. [[CrossRef](#)]
84. Henry, D.J.; Dutrow, B.L. Tourmaline at diagenetic to low-grade metamorphic conditions: Its petrologic applicability. *Lithos* **2012**, *154*, 16–32. [[CrossRef](#)]
85. Berryman, E.J.; Wunder, B.; Ertl, A.; Koch-Müller, M.; Rhede, D.; Scheidl, K.; Giester, G.; Heinrich, W. Influence of the X-site composition on tourmaline's crystal structure: Investigation of synthetic K-dravite, dravite, oxy-uvite, and magnesio-foitite using SREF and Raman spectroscopy. *Phys. Chem. Miner.* **2015**, *43*, 83–102. [[CrossRef](#)]
86. Dutrow, B.L.; Henry, D.J. Fibrous tourmaline: A sensitive probe of fluid compositions and petrologic environments. *Can. Mineral.* **2016**, *54*, 311–335. [[CrossRef](#)]
87. Mercadier, J.; Richard, A.; Cathelineau, M. Boron- and magnesium-rich marine brines at the origin of giant unconformity-related uranium deposits: δ¹¹B evidence from Mg-tourmalines. *Geology* **2012**, *40*, 231–234. [[CrossRef](#)]
88. Biernacka, J. Insight into diagenetic processes from authigenic tourmaline: An example from Carboniferous and Permian siliciclastic rocks of western Poland. *Sediment. Geol.* **2019**, *389*, 73–90. [[CrossRef](#)]
89. Berryman, E.J.; Kutzschbach, M.; Trumbull, R.B.; Meixner, A.; van Hinsberg, V.; Kasemann, S.A.; Franz, G. Tourmaline as a petrogenetic indicator in the Pfitsch Formation, Western Tauern Window, Eastern Alps. *Lithos* **2017**, *284–285*, 138–155. [[CrossRef](#)]

90. Thomson, J.A. A rare garnet-tourmaline-sillimanite-biotite-ilmenite-quartz assemblage from the granulite-facies region of south-central Massachusetts. *Am. Mineral.* **2006**, *91*, 1730–1738. [[CrossRef](#)]
91. Ertl, A.; Marschall, H.R.; Glester, G.; Henry, D.J.; Schertl, H.P.; Ntaflos, T.; Luvizotto, G.L.; Nasdala, L.; Tillmanns, E. Metamorphic ultrahigh-pressure tourmaline: Structure, chemistry, and correlations to P-T conditions. *Am. Mineral.* **2010**, *95*, 1–10. [[CrossRef](#)]
92. Shimizu, R.; Ogasawara, Y. Diversity of potassium-bearing tourmalines in diamondiferous Kokchetav UHP metamorphic rocks: A geochemical recorder from peak to retrograde metamorphic stages. *J. Asian Earth Sci.* **2013**, *63*, 39–55. [[CrossRef](#)]

Disclaimer/Publisher’s Note: The statements, opinions and data contained in all publications are solely those of the individual author(s) and contributor(s) and not of MDPI and/or the editor(s). MDPI and/or the editor(s) disclaim responsibility for any injury to people or property resulting from any ideas, methods, instructions or products referred to in the content.